Inorg. Chem. **2007**, *46*, 3705–3713

Isostructural *neo*-Pentoxide Derivatives of Group 3 and the Lanthanide Series Metals for the Production of Ln_2O_3 Nanoparticles

Timothy J. Boyle,* Leigh Anna M. Ottley, Sherrika D. Daniel-Taylor, Louis J. Tribby, and Scott D. Bunge[†]

Sandia National Laboratories, Advanced Materials Laboratory, 1001 University Boulevard, SE, Albuquerque, New Mexico 87106

Alison L. Costello and Todd M. Alam

Sandia National Laboratories, New Mexico, P.O. Box 5800, Albuquerque, New Mexico 87185-0886

John C. Gordon and T. Mark McCleskey

Chemistry Division and Materials Physics Application Division, Los Alamos National Laboratory, MS J514, Los Alamos, New Mexico 87545

Received February 8, 2007

The synthesis and characterization of a series of *neo*-pentoxide ($OCH_2C(CH_3)_3$ or ONep) derivatives of group 3 and the lanthanide (Ln) series' metals were undertaken via an amide/alcohol exchange route. Surprisingly, the products isolated and characterized by single-crystal X-ray diffraction yielded isostructural species for every trivalent cation studied: $[Ln(\mu\text{-ONep})_2(ONep)]_4$ [Ln = Sc (**1**), Y (**2**), La (**3**), Ce (**4**), Pr (**5**), Nd (**6**), Sm (**7**), Eu (**8**), Gd (**9**), Tb (**10**), Dy (**11**), Ho (**12**), Er (**13**), Tm (**14**), Yb (**15**), Lu (**16**)]. Compounds **3**, **4**, **6**, and **11** have been previously reported. Within this series of complexes, the Ln metal centers are oriented in a square with each Ln–Ln edge interconnected via two μ-ONep ligands; each metal center also binds one terminal ONep ligand. NMR data of **1**–**3** indicate that the solid-state structure is retained in solution. FTIR spectroscopy (KBr pellet) revealed the presence of significant Ln– – –H–C interactions within one set of the bridging ONep ligands in all cases; the stretching frequencies of these C–H bonds appear to increase in magnitude with decrease in metal ion radius. These complexes were used to generate nanoparticles through solution hydrolysis routes, resulting in the formation of lanthanide oxide nanoparticles and rods. The emission properties of these ceramics were preliminarily investigated using UV–vis and PL measurements.

Introduction

The use of lanthanide (Ln) elements in materials syntheses has recently gained increased attention.[1−3] The systematic decrease in radius across the series while maintaining the +3 ionic charge is one reason these cations are of interest—an overall decrease of more than 0.18 Å is calculated for hexacoordinated Ln cations.[4] As a result of this controlled variability, the properties of Ln-containing ceramic materials can be "fine-tuned" by the radius of the trivalent Ln cation. This was demonstrated, for example, in our study of the ferroelectric, Ln-doped PZT materials (PLnZT), where the polarization, dielectric constant, and fatigue resistance were found to be significantly improved with the inclusion of aliovalent cations.[5,6]

* To whom correspondence should be addressed. Phone: (505)272-7625. Fax: (505)272-7336. E-mail: tjboyle@Sandia.gov.

[†] Current address: Department of Chemistry, Kent State University, 305 Williams Hall, Kent, OH 44242-0001.

(1) Bradley, D. C.; Mehrotra, R. C.; Gaur, D. P. *Metal Alkoxides*; Academic Press: New York, 1978.

(2) Bradley, D. C.; Mehrotra, R. C.; Rothwell, I. P.; Singh, A. *Alkoxo and Aryloxo Derivatives of Metals*; Academic Press: New York, 2001; p 704.

(3) Turova, N. Y.; Turevskaya, E. P.; Kessler, V. G.; Yanovskaya, M. I. *The Chemistry of Metal Alkoxide*; Kluwer Academic Publishers: Boston, 2002; p 568.

(4) Shannon, R. D. *Acta. Crystallogr., Sect. A: Found. Crystallogr.* **1976**, *A32*, 751.

10.1021/ic070253u CCC: $37.00
Published on Web 03/27/2007

Metal alkoxides ($M(OR)_x$) are excellent precursors for the production of ceramic materials as a result of their low thermal decomposition temperatures, readily adjustable solubility and volatility, and commercial availability. Conveniently, the structure of $M(OR)_x$ precursors can often be controlled through a variety of modifying ligands. It is well documented that the atomic connectivity of a specific molecular precursor will have a pronounced effect on the properties of the resulting ceramic phase(s) derived from it. Therefore, it is critical to understand the structural characteristics of these molecular precursors. Surprisingly, a search of the literature revealed only a few structurally characterized examples of homoleptic lanthanide alkoxide complexes. Furthermore, there appear to be no examples of (the same) alkoxide ligands supporting complexes containing metals across the entire 4f-series.[1−3,6−8]

For a given ligand set, changes in coordination number and the final geometry may occur as a result of the Ln contraction (as observed by one or more structural changeover points within the series). In addition, trivalent Sc represents a relatively small ion in comparison to those of the lanthanide series, and it is reported that Sc containing species are expected to resemble Al in their chemistry more than those of the lanthanides.[9] However, no systematic structural study of molecules containing group 3 metals and the entire lanthanide series supported *by the same single* alkoxide ligand set is available to verify these statements.

One ligand that we have reported to be of utility in generating high quality ceramic materials is the *neo*-pentoxide ($OCH_2C(CH_3)_3$ = ONep) moiety.[10−12] A literature search, prior to this study, revealed only two reports of structurally characterized homoleptic "$Ln(ONep)_3$" derivatives both of which adopt a tetrameric structure, $[Ln(\mu\text{-}ONep)_2(ONep)]_4$ (Ln = La, Nd).[8a] Both La and Nd occur early in the Ln series and thus represent trivalent members possessing larger ionic radii. The Dy[6] and Ce[8b] adducts were recently reported by us to also adopt the same tetranuclear core. We therefore decided to explore and extend these investigations to include the entire Ln series as well as the group 3 cations (i.e., Sc and Y) in order to determine what effect that the diminishing ionic radius might have on the final molecular structure of this "$Ln(ONep)_3$" series where Ln = Sc (**1**), Y (**2**), La (**3**),[8a] Ce (**4**),[8b] Pr (**5**), Nd (**6**),[8a] Sm (**7**), Eu (**8**), Gd (**9**), Tb (**10**), Dy (**11**),[6] Ho (**12**), Er (**13**), Tm (**14**), Yb (**15**), and Lu (**16**). Although compounds **3**,[8a] **4**,[8b] **6**,[8a] and **11**[6] were previously reported, crystals were again isolated and the structures resolved, yielding identical results to the literature reports. These examples are therefore not discussed in detail in this report. In each case, FTIR spectroscopy revealed that significant Ln− − −H−C agostic interactions were present. The synthesis, structural properties, and relevant spectroscopic data are reported below. Having this unique set of isostructural compounds now available to us, we elected to investigate the influence that the presence of cations have on the final morphology and properties of nanoparticles of Ln_2O_3.

Experimental Section

All compounds described below were handled with rigorous exclusion of air and water using standard Schlenk line and glovebox techniques. All reactions were run under an argon atmosphere in a glovebox. All solvents were stored under argon and used as received (Aldrich) in sure seal bottles, including hexanes (hex), toluene (tol), tetrahydrofuran (THF), and diethyl ether (Et_2O). The following chemicals were used as received (Aldrich and Alfa Aesar): $ScBr_3$, YCl_3, $CeBr_3$, $PrBr_3$, $SmBr_3$, $EuCl_3$, $GdCl_3$, $TbCl_3$, $HoCl_3$, $ErCl_3$, $TmCl_3$, YCl_3, $LuCl_3$, ANR_2 [A = Li, K; R = $Si(CH_3)_3$]. $Ln(NR_2)_3$ (Ln = Sc, Y, Ce, Pr, Sm, Eu, Gd, Tb, Ho, Er, Tm, Yb, and Lu) were synthesized through the reaction of LnX_3 and 3 equiv of ANR_2 in THF or Et_2O.[1−3]

FT−IR data were obtained on a Bruker Vector 22 Instrument using KBr pellets under an atmosphere of flowing nitrogen. Elemental analysis was performed on a Perkin-Elmer 2400 CHN−S/O elemental analyzer.

All NMR samples were prepared from dried crystalline materials that were handled and stored under an argon atmosphere and redissolved in toluene-d_8/1%TMS. The solution ^1H NMR spectra were obtained on a Bruker DRX400 at 399.87 MHz using standard conditions at RT.

Synthesis of $[Ln(\mu\text{-}ONep)_2(ONep)]_4$. Due to the similarity of syntheses of **1**−**16**, a general description is supplied for this set of compounds. A hexane solution of H-ONep (∼5 mL) was added dropwise to a vial containing a solution of the appropriate $Ln(NR_2)_3$ complex in ∼15 mL of hexane. After stirring, the resultant clear reaction mixture concentrated by rotary evaporation and then either cooled at −35 °C or left at room temperature until X-ray quality crystals formed.

$[Sc(\mu\text{-}ONep)_2(ONep)]_4$ (1). $Sc[NR_2]_3$ (0.460 g, 0.870 mmol) and H-ONep (0.230 g, 2.61 mmol) were used. Yield: 0.210 g (78.3%). FTIR: (KBr, cm^{-1}) 2955(s), 2906(s), 2867(m), 2698(w), 1560(w), 1479(m), 1459(m), 1420(s), 1397(m), 1363(m), 1261(s), 1154(m), 1094(m), 1020(s), 802(s), 669(m), 577(w), 464(m), 455(m). Elemental analysis Calc'd for $C_{60}H_{132}O_{12}Sc_4$: 58.80 %C, 10.86 %H. Found: 54.86 %C, 10.29 %H.

$[Y(\mu\text{-}ONep)_2(ONep)]_4$ (2). $Y[NR_2]_3$ (0.500 g, 0.880 mmol) and H-ONep (0.232 g, 0.877 mmol) were used. Yield: 0.180 g (58.0%). FTIR: (KBr, cm^{-1}) 2975(s), 2943(w, sh), 2861(m), 2820(w, sh), 2687(w), 2364(w), 2328(w), 1477(s), 1466(m, sh), 1384(m), 1354(m), 1261(w), 1200(w, sh), 1129(s), 1056(s), 1015(s), 936(m), 905(m), 823(w), 751(m), 669(w, sh), 597(m, sh), 556(s), 423(s). Elemental analysis Calc'd for $C_{60}H_{132}O_{12}Y_4$: 51.43 %C; 9.35 %H. Found: 49.13 %C, 8.78 %H.

$[La(\mu\text{-}ONep)_2(ONep)]_4$ (3). See ref 8a.

(5) Boyle, T. J.; Clem, P. G.; Tuttle, B. A.; Brennecka, G. L.; Dawley, J. T.; Rodriguez, M. A.; Dunbar, T. D.; Hammetter, W. F. *J. Mater. Res.* **2002**, *17*, 871.

(6) Boyle, T. J.; Bunge, S. D.; Clem, P. G.; Richardson, J.; Dawley, J. T.; Ottley, L. A. M.; Rodriguez, M. A.; Tuttle, B. A.; Avilucea, G.; Tissot, R. G. *Inorg. Chem.* **2005**, *44*, 1588.

(7) Deacon, G. B.; Feng, T.; Nickel, S.; Ogden, M. I.; White, A. H. *Aust. J. Chem.* **1992**, *45*, 671.

(8) (a) Barnhart, D. M.; Clark, D. L.; Gordon, J. C.; Huffman, J. C.; Watkin, J. G.; Zwick, B. D. *J. Am. Chem. Soc.* **1993**, *115*, 8461. (b) Boyle, T. J.; Tribby, L. J.; Bunge, S. D. *Eur. J. Inorg. Chem.* **2006**, 4553.

(9) Cotton, F. A.; Wilkinson, G. *Advanced Inorganic Chemistry*, 5th ed.; John Wiley & Sons: New York, 1988.

(10) Boyle, T.; Alam, T.; Mechenbier, E.; Scott, B.; Ziller, J. *Inorg. Chem.* **1997**, *36*, 3293.

(11) Boyle, T. J.; Gallegos, J. J. I.; Pedrotty, D. M.; Mechenbeir, E. R.; Scott, B. *Coord. Chem.* **1999**, *47*, 155.

(12) Boyle, T. J.; Alam, T. M.; Dimos, D.; Moore, G. J.; Buchheit, C. D.; Al-Shareef, H. N.; Mechenbeir, E. R.; Bear, B. R.; Ziller, J. W. *Chem. Mater.* **1997**, *9*, 3187.

[Ce(μ-ONep)$_2$(ONep)]$_4$ (4).[8b] Ce[NR$_2$]$_3$ (0.221 g, 0.320 mmol) and H-ONep (0.094 g, 1.10 mmol) were used. Yield: 0.088 g (62.0%). FTIR: (KBr, cm^{-1}) 2951(s), 2864(s), 2803(s), 2687(m), 1478(s), 1460(m), 1391(m), 1359(m), 1255(w), 1216(w), 1107(s), 1060(s), 1019(s), 933(m), 897(m), 750(m), 702(m), 592(s), 561(m, sh), 426(m). Elemental analysis calc'd for $C_{60}H_{132}Ce_4O_{12}$: 44.87 %C, 8.32 %H. Found: 44.67 %C, 8.17 %H.

[Pr(μ-ONep)$_2$(ONep)]$_4$ (5). Pr[NR$_2$]$_3$ (1.00 g, 1.61 mmol) and H-ONep (0.425 g, 4.82 mmol) were used. Yield: 0.452 g (68.5%). FTIR: (KBr, cm^{-1}) 2962(s), 2905(m), 2862(m), 2823(m), 2692(m), 2642(w), 1604(m), 1572(w), 1556(w), 1479(m), 1439(m), 1269(s), 1089(s), 1045(s, sh), 1019(s), 934(w), 862(m, sh), 725(s), 724(w, sh), 703(m), 664(w, sh), 645(m), 599(m), 556(m). Elemental analysis calc'd for $C_{60}H_{132}Pr_4O_{12}$ 44.78 %C; 8.14 %H. Found: 44.39 %C, 8.04 %H.

[Nd(μ-ONep)$_2$(ONep)]$_4$ (6). See ref 8a.

[Sm(μ-ONep)$_2$(ONep)]$_4$ (7). Sm[NR$_2$]$_3$ (0.500 g, 0.790 mmol) and H-ONep (0.210 g, 0.793 mmol) were used. Yield: 0.290 g (74.4%). FTIR: (KBr, cm^{-1}) 2963(s), 2905(m), 2824(w), 2697(w), 2662(w), 2500(w) 1943(w), 1604(m), 1479(w) 1438(m), 1413(m), 1362(m), 1261(s), 1091(s), 1020(s), 934(w), 863(w, sh), 799(s), 727(w), 702(m), 695(m), 645(m), 553(m), 464(w). Elemental analysis calc'd for $C_{60}H_{132}O_{12}Sm_4$: 43.75 %C, 8.08 %H. Found: 43.31 %C, 8.44 %H.

[Eu(μ-ONep)$_2$(ONep)]$_4$ (8). Eu[NR$_2$]$_3$ (0.500 g, 0.790 mmol) and H-ONep (0.209 g, 0.791 mmol) were used. Yield: 0.211 g (63.9%). FTIR: (KBr, cm^{-1}) 2963(s), 2905(s), 2812(m), 2697(w), 2662(m), 2052(m), 1996(m, sh), 1944(m), 1770(w), 1716(w), 1697(w), 1604(m), 1496(w), 1479(m, sh), 1445(s), 1412(s), 1364(w), 1260(s), 1989(s), 1019(s), 798(s), 728(w), 695(s), 664(s), 608(w, sh), 608(w), 555(m), 502(m), 464(w, sh). Elemental analysis calc'd for $C_{60}H_{132}Eu_4O_{12}$: 43.58 %C, 7.92 %H. Found: 43.20 %C, 7.60 %H.

[Gd(μ-ONep)$_2$(ONep)]$_4$ (9). Gd[NR$_2$]$_3$ (1.00 g, 1.56 mmol) and H-ONep (0.410 g, 4.73 mmol) were used. Yield: 0.41 g (62.4%). FTIR: (KBr, cm^{-1}) 2962(s), 2905(s), 2869(m), 2811(m), 2715(w), 2697(w), 2661(w), 1944(w), 1600(w), 1479(m), 1446(m), 1413(s), 1362(m), 1260(s), 1091(s), 932(s), 866(m), 798(s), 699(m), 665(m), 605(m), 565(w), 502(w), 415(w). Elemental analysis calc'd for $C_{60}H_{132}O_{12}Gd_4$: 43.04 %C, 7.89 %H. Found: 42.26 %C, 7.56 %H.

[Tb(μ-ONep)$_2$(ONep)]$_4$ (10). Tb[NR$_2$]$_3$ (1.00 g, 1.56 mmol) and H-ONep (0.413 g, 4.69 mmol) were used. Yield: 0.594 g (89.6%). FTIR: (KBr, cm^{-1}) 2963(s), 2905(m), 2868(w), 2818(w), 2718(w), 2701(w), 2663(w), 1944(w), 1603(w), 1478(m), 1445(m), 1413(s), 1361(m), 1259(s), 1094(s), 934(s), 864(s), 800(s), 701(m), 688(m), 663(m), 615(w), 560(w), 500(w). Elemental analysis calc'd for $C_{60}H_{132}O_{12}Tb_4$: 42.61 %C, 7.89 %H. Found: 42.17 %C, 7.58 %H.

[Dy(μ-ONep)$_2$(ONep)]$_4$ (11). See ref 6.

[Ho(μ-ONep)$_2$(ONep)]$_4$ (12). Ho[NR$_2$]$_3$ (1.00 g, 1.55 mmol) and H-ONep (0.400 g, 4.50 mmol) were used. Yield: 0.302 g (45.3%). FTIR: (KBr, cm^{-1}) 2963(s), 2905(s), 2814(m), 2743(w), 2718(w), 2670(m), 2662(w), 2612(w), 2575(w), 1946(m), 1599(m), 1478(m, sh), 1445(m), 1412(m), 1360(m), 1261(s), 1093(s), 1021(s), 932(w), 864(m, sh), 799(s), 755(m, sh), 702(m), 68(m), 663(m), 611(w), 568(m), 558(m), 498(m). Elemental analysis calc'd for $C_{60}H_{132}Ho_4O_{12}$: 42.26 %C, 7.74 %H. Found: 42.71 %C, 7.88 %H.

[Er(μ-ONep)$_2$(ONep)]$_4$ (13). Er[NR$_2$]$_3$ (0.500 g, 1.54 mmol) and H-ONep (0.408 g, 4.63 mmol) were used. Yield: 0.250 g (83.3%). FTIR: (KBr, cm^{-1}) 2958(s), 2904(s, sh), 2866(m), 2837(w), 2702(w), 2364(w), 2345(w), 1471(s), 1461(s, sh), 1394(s), 1363(s), 1255(m), 1214(w), 1122(s), 1056(s), 1019(s), 931(m), 984(m), 750(m), 699(w), 608(s), 560(m), 420(m). Elemental analysis calc'd for $C_{60}H_{132}Er_4O_{12}$: 42.03 %C, 7.64 %H. Found: 41.36 %C, 7.32 %H.

[Tm(μ-ONep)$_2$(ONep)]$_4$ (14). Tm[NR$_2$]$_3$ (1.00 g, 1.54 mmol) and H-ONep (0.407 g, 4.61 mmol) were used. Yield: 0.594 g (88.4%). FTIR: (KBr, cm^{-1}) 2955(s), 2865(m, sh), 2696(w), 1480(s), 1463(m, sh), 1393(m), 1364(m), 1327(m), 1260(m), 1126(s), 1056(s), 1017(s), 932(w), 897(w), 804(m), 551(w), 608(s), 573(w, sh), 480(w), 421(w). Elemental analysis calc'd for $C_{60}H_{132}O_{12}Tm_4$: 41.86 %C, 7.68 %H. Found: 41.59 %C, 7.58%H.

[Yb(μ-ONep)$_2$(ONep)]$_4$ (15). Yb[NR$_2$]$_3$ (1.00 g, 1.53 mmol) and H-ONep (0.404 g, 4.59 mmol) were used. Yield: 0.100 g (81.6%). FTIR: (KBr, cm^{-1}) 2960(s), 2905(s), 2869(m), 2818(m), 2721(w), 2702(w), 2663(w), 1944(w), 1600(w), 1477(m), 1446(m), 1413(s), 1362(m), 1263(s), 1094(s), 935(s), 864(m), 797(s), 701(m), 688(m), 663(m), 616(w), 447(w). Elemental analysis calc'd for $C_{66}H_{146}O_{12}Yb_4$: 41.47 %C, 8.07 %H. Found: 41.50 %C, 7.60 %H.

[Lu(μ-ONep)$_2$(ONep)]$_4$ (16). Lu[NR$_2$]$_3$ (1.00 g, 1.52 mmol) and H-ONep (0.403 g, 4.57 mmol) were used. Yield: 0.520 g (78.2%). FTIR: (KBr, cm^{-1}) 2962(s), 2905(s), 2867(m), 2742(m), 2724(w), 2702(w), 2664(w), 1946(w), 1600(w), 1479(m), 1446(m), 1412(s), 1362(m), 1263(s), 1106(s), 934(s), 864(m), 796(s), 702(m), 688(m), 664(m), 573(w), 560 (w), 499(w). Elemental analysis calc'd for $C_{66}H_{146}Lu_4O_{12}$: 41.24 %C, 7.56 %H. Found: 41.94 %C, 7.90 %H.

General X-ray Crystal Structure Information.[13] Each crystal was mounted onto a thin glass fiber from a pool of Fluorolube and immediately placed under a liquid N_2 stream, on a Bruker AXS diffractometer. The radiation used was graphite monochromatized Mo Kα radiation (λ = 0.7107 Å). The lattice parameters were optimized from a least-squares calculation on carefully centered reflections. Lattice determination and data collection were carried out using SMART Version 5.054 software. Data reduction was performed using SAINT Version 6.01 software. The structure refinement was performed using XSHELL 3.0 software. The data were corrected for absorption using the SADABS program within the SAINT software package.

It is of note that crystal structures of metal alkoxides are often plagued by disorder within the atoms of the ligand chain. This phenomenon subsequently leads to larger *R*-values. Each structure was solved using direct methods. This procedure yielded the heavy atoms, along with a number of the C and O atoms. Subsequent Fourier synthesis yielded the remaining atom positions. Noncentrosymmetric settings were chosen for all structures even though a mirror plane appears to exist for these molecules. By further investigation of these species, disruption in the symmetry due to nonrigid ONep ligands ultimately requires refinement in noncentrosymmetric settings. Final crystal solutions of the ONep ligands of **9**, **10**, and **12** show significant translational disorder which is often noted for this family of compounds. Attempts were made to model this disorder by distributing the positions of the C over several sites. These attempts proved fruitless as the disorder does not display clearly defined positions for the partial occupied sites. Hence, these attempts were abandoned in favor of one large thermal ellipsoid for many of the OR ligands in these structures. For all solutions, the central core connectivities were unequivocally established. X−H bonds were not included in the refinement of the final structure of **9**, **2**, **14**, and **15**. For **4**[8b] and **8** toluene solvent molecules were squeezed out of the structure using Platon squeeze methods in order to improve refinement and establish the con-

(13) Yanovsky, A. I.; Turova, N. Y.; Turevskaya, E. P.; Kessler, V. G.; Struchkov, Y. T. *Zh. Neorg. Khim. Russ. Russ. J. Inorg. Chem.* **1993**, *38*, 779.

Table 1. Data Collection Parameters for **1**−**16**

compound	**1**	**2**	**4**[8b]	**5**	**7**	**8**	**9**
chemical formula	$C_{66}H_{139}O_{12}Sc_4$	$C_{60}H_{132}O_{12}Y_4$	$C_{116}H_{196}Ce_4O_{12}$	$C_{67}H_{140}O_{12}Pr_4$	$C_{60}H_{132}O_{12}Sm_4$	$C_{60}H_{132}Eu_4O_{12}$	$C_{60}H_{132}Gd_4O_{12}$
formula weight	1304.61	1401.30	2343.21	1701.43	1647.06	1653.50	1674.66
temp (K)	233(2)	178(2)	168(2)	203(2)	203(2)	203(2)	203(2)
space group	tetragonal *P*-42(1)*c*	tetragonal *P*-42(1)*c*	tetragonal *P*-42(1)*c*	tetragonal *P*-42(1)*c*	tetragonal *P*-42(1)*c*	tetragonal *P*-42(1)*c*	tetragonal *P*-42(1)*c*
a (Å)	20.170(2)	18.034(2)	20.5590(18)	20.7040(13)	18.2051(18)	20.4403(8)	18.367(3)
b (Å)	20.170(2)	18.034(2)	20.5590(18)	20.7040(13)	18.2051(18)	20.4403(8)	18.367(3)
c (Å)	11.844(3)	11.773(3)	11.908(2)	11.9418(15)	11.749(2)	12.0304(9)	11.927(4)
V (Å^3)	4818.1(13)	3829.1(11)	5033.1(11)	5118.9(8)	3894.0(9)	5026.4(5)	4023.5(18)
Z	2	2	2	2	2	2	2
D_{calcd} (Mg/m^3)	0.899	1.215	1.546	1.104	1.405	1.093	1.382
μ (Mo, Kα) (mm^{-1})	0.310	3.048	1.838	1.909	3.018	2.497	3.299
R1[a] (%) (all data)	4.52 (5.05)	3.70(5.01)	4.60 (9.09)	3.95 (4.33)	6.21 (7.82)	2.70 (2.82)	4.54 (6.01)
wR2[b] (%) (all data)	12.98 (13.28)	8.97(9.59)	6.49 (9.59)	10.88 (11.07)	11.52 (12.06)	7.63 (7.70)	12.22 (13.63)

compound	**10**	**11**[6]	**12**	**13**	**14**	**15**	**16**
chemical formula	$C_{60}H_{132}O_{12}Tb_4$	$C_{60}H_{132}Dy_4O_{12}$	$C_{60}H_{132}Ho_4O_{12}$	$C_{66}H_{146}Er_4O_{12}$	$C_{60}H_{132}O_{12}Tm_4$	$C_{66}H_{146}O_{12}Yb_4$	$C_{66}H_{146}Lu_4O_{12}$
formula weight	1681.34	1695.66	1705.38	1800.87	1721.38	1823.99	1831.71
temp (K)	203(2)	168(2)	203(2)	168(2)	203(2)	168(2)	168(2)
space group	tetragonal *P*-42(1)*c*	tetragonal *P*-42(1)*c*	tetragonal *P*-42(1)*c*	tetragonal *P*-42(1)*c*	tetragonal *P*-42(1)*c*	tetragonal *P*-42(1)*c*	tetragonal *P*-42(1)*c*
a (Å)	18.1060(6)	18.0322(6)	18.0400(12)	20.1985(14)	20.2106(17)	20.2960(9)	20.304(3)
b (Å)	18.1060(6)	18.0322(6)	18.0400(12)	20.1985(14)	20.2106(17)	20.2960(9)	20.304(3)
c (Å)	11.7612(7)	11.7258(7)	11.7617(15)	12.0226(16)	12.048(2)	11.789(10)	11.772(2)
V (Å^3)	3855.6(3)	3812.8(3)	3827.7(6)	4905.0(8)	4920.1(10)	4860.3(5)	4853.0(12)
Z	2	2	2	2	2	2	2
D_{calcd} (Mg/m^3)	1.448	1.477	1.480	1.219	1.159	1.246	1.253
μ (Mo, Kα) (mm^{-1})	3.671	3.922	4.136	3.427	3.608	3.853	4.073
R1[a] (%) (all data)	2.57 (2.71)	3.85 (4.81)	6.15 (6.60)	2.82 (3.32)	4.96 (5.58)	3.03 (3.32)	3.05 (3.54)
wR2[b] (%) (all data)	6.29 (6.39)	7.63 (7.90)	9.76 (9.89)	7.36 (7.51)	18.02 (18.67)	8.05 (8.18)	7.53 (7.70)

[a] $R_1 = \sum||F_o| - |F_c||/\sum|F_o| \times 100$. [b] $wR_2 = [\sum w(F_o^2 - F_c^2)^2/\sum(w|F_o|^2)^2]^{1/2} \times 100$.

nectivity. This manipulation causes some discrepancies for the calculated molecular weight. Specific information can be found in the Supporting Information. For those compounds that had H−X included, the hydrogen atoms were fixed in positions of ideal geometry and refined within the XSHELL software. These idealized hydrogen atoms had their isotropic temperature factors fixed at 1.2 or 1.5 times the equivalent isotropic U of the C atoms to which they were bonded. The final refinement of each compound included anisotropic thermal parameters on all non-hydrogen atoms. Additional information concerning the data collection and final structural solutions (Table 1) of these compounds can be found in the Supporting Information or by accessing CIF files through the Cambridge Crystallographic Data Base.

Nanoparticle Synthesis. In order to explore morphological variations within different ceramic nanoparticles produced during hydrolysis, (i.e., those wrought by the changes in the nature of the cation), a representative set of precursors containing early, middle, and late members of the 4f-series were studied. 1-Methylimidazole and water (MeIm/H_2O at 14.5:0.5 mL) were mixed in a 3-neck round-bottom flask, equipped with a septum, reflux condenser, and a gas adapter, and heated to reflux temperature (∼180 °C).[14,15] An ∼0.4 M solution of the appropriate Ln(OR)$_3$/hexanes stock solution was drawn into a syringe (3.0 mL) in the glovebox, transferred to the Schlenk line, and rapidly injected (∼ 1.0 s) into the heated MeIm/H_2O solution. The resulting mixture was refluxed for 2 h. After the solution was cooled, centrifuged, and decanted, the lanthanide oxide particles were precipitated using isopropyl alcohol (H−OPr^i). The precipitated particles were washed twice with H−OPr^i.

The nanoparticles were characterized using Transmission Electron Microscopy (TEM) by taking an aliquot of the desired precipitate suspended in hexanes and placing it directly onto a carbon-coated copper transmission electron microscopy (TEM) grid (300 mesh) purchased from Electron Microscopy Sciences. The aliquot was then allowed to dry. The resultant particles were studied using a Philips CM 30 TEM operating at 300-kV accelerating voltage. The various nanoparticles were also characterized by Powder X-ray Diffraction (XRD). The XRD patterns of the materials were obtained on a Siemens 5D500 diffractometer using Cu KR radiation, excited at 40 kV and 30 mA. The X-rays were collimated at the source with 1° divergence scatter slits with a detector that had 1° scatter and receiving slits using a graphite diffracted beam monochromator.

Photoluminescence Measurements. For each of the different nanoparticle phases generated above, a photoluminescence (PL) measurement was obtained to probe its fluorescent behavior. A suspension of Ln_2O_3 nanoparticles was placed onto a quartz microscope slide by pipet and allowed to dry overnight. The resultant samples were studied using a Spex Fluorlog-2 Flourometer. Spectra of Ln_2O_3 (**1**, **2**, **5**, **11**) were investigated on films using front face configuration under 275 nm (Xe lamp) excitation.

UV−vis Spectroscopy. UV−vis absorption spectra were collected at room temperature on a Varian Carey 400 spectrophotometer. Each aliquot was quenched directly in a UV cell containing toluene. The spectra were collected from 800 to 200 nm with a scan rate of 0.5 nm per minute.

MicroXRD. MicroXRD analysis was performed using a Bruker D8 diffractometer with a 1 mm collimator and incident beam Goebel mirror. Scans are typically collected from 5 to 60°, 2θ at 0.04° steps at 2 min per step using Cu Ka radiation at 40 kV 40 mA.

Magnetic Moment Measurements. Evans Method. The solution ^{1}H NMR spectrum was obtained on a Bruker DRX400 at 399.87 MHz using standard conditions at RT. For the Evans

(14) Boyle, T. J.; Rodriguez, M. A.; Ingersoll, D.; Headley, T. J.; Bunge, S. D.; Pedrotty, D. M.; De'Angeli, S. M.; Vick, S. C.; Fan, H. *Chem. Mater.* **2002**, *15*, 3903.
(15) Boyle, T. J.; Bunge, S. D.; Andrews, N. L.; Matzen, L. E.; Sieg, K.; Rodriguez, M. A.; Headley, T. J. *Chem. Mater.* **2004**, *16*, 3279.

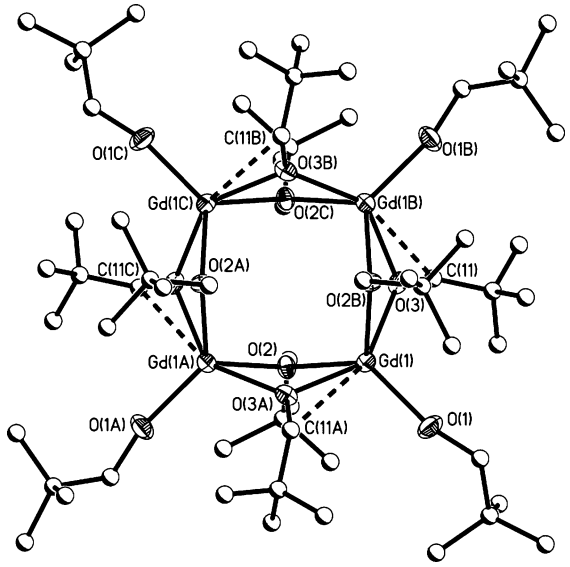

Figure 1. Structure plot of $[Gd(\mu\text{-ONep})_2(ONep)]_4$ (**9**). Heavy atoms thermal ellipsoids drawn at the 30% level and carbon and hydrogen atoms drawn as ball and stick for simplicity. All derivatives have similar arrangements.

method,[16−18] the chemical shifts were referenced to the TMS chemical shift in the solvent (toluene-d_8/1% TMS). Magnetic susceptibilities were determined using the difference in the observed chemical shift of the internal reference (TMS) with and without the paramagnetic substance using a coaxial NMR tube.

Results and Discussion

No report detailing an isostructural series of trisalkoxy lanthanide ($Ln(OR)_3$) complexes is readily available in the literature. As previously mentioned, we were interested in exploring a series of structurally characterized homoleptic "$Ln(ONep)_3$" precursors potentially capable of producing tailored ceramic nanomaterials. The ONep ligand is of interest due to the ease with which complexes supported by this ligand can be crystallized and as a result of the fact that this moiety also confers desirable molecular decomposition pathways that are favorable for materials synthesis properties. Therefore, we undertook the synthesis, characterization, and manipulation of these to form a series of Ln_2O_3 nanoceramics. The results of these investigations including characterization of the molecular precursors, the observed trends, and materials produced are presented below.

Synthesis. The syntheses of complexes **1**−**16** were achieved using an amide/alcohol exchange reaction shown in eq 1.[1−3] In a general synthetic route, a solution of H-ONep dissolved in hexanes was slowly added to the appropriate hexanes solution of $Ln(NR_2)_3$. After stirring for a short period of time, the reaction was allowed to sit unsealed until sufficient solvent evaporation had occurred and X-ray quality crystals formed. In the cases where crystals did not grow, the reaction mixture was dried to a powder by rotary evaporation. The powder was redissolved in hexanes, and X-ray quality crystals were isolated through slow evaporation of the volatile material.

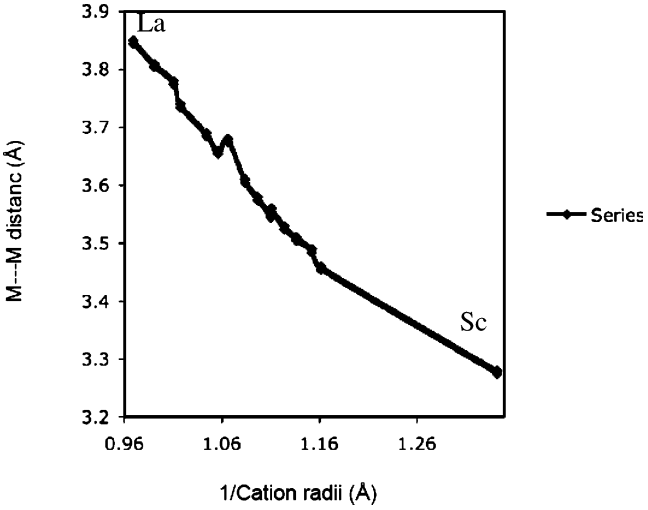

Figure 2. Plot of central void size (Å) versus the radii size (1/Å). Plot of M−M void versus 1/cation radii.

$$Ln(NR_2)_3 + 3.0\text{H-ONep} \xrightarrow{\text{hex}} [Ln(\mu\text{-ONep})_2(ONep)]_4 + 3\text{H}-NR_2 \quad (1)$$

The resulting crystals were found to be colorless except in the cases of the following cations (pale color): Ce (yellow),[8b] Nd (blue),[8a] Sm (yellow), Er (pink). Elemental analyses of each sample in general were consistent with the empirical formula "$Ln(OR)_3$". Analytical results for compounds derived from the smaller cations (Sc and Y) deviated most from calculated values. This technique relies on complete combustion of the compound followed by analyses of the resultant gases which can be difficult for volatile species (as was noted for other early transition metal ONep ligated species such as $[Ti(\mu\text{-ONep})(ONep)_3]_2$[10]).

X-ray Structures. In order to verify the intimate connectivities of these compounds, single-crystal X-ray diffraction studies were undertaken. Rather surprisingly, since a change in cation size from La^{+3} to Sc^{+3} is greater than 0.28 Å,[4] each of the Ln complexes crystallized in this study and those derivatives from the previous literature reports[6,8] (16 total compounds) were found to be isostructural, isolated in the tetragonal $P\text{-}42_1c$ space group. Only the La adduct was solved in the orthorhombic $P2_12_12$ space group.[8a] While this crystallization habit did not change the molecular structure, it is most likely a reflection of the amount and type of solvent that cocrystallized within the lattice of the La derivative. The exceptionally high quality of these structural solutions is unusual for metal alkoxide complexes which are often plagued with disorder due to multiple orientations of the hydrocarbon chains of the ligands. This quality allows us to discuss metrical data of **1**−**16** in some detail.

For **1**−**16**, the metal centers are oriented in a square arrangement and interconnected via eight bridging μ-ONep ligands (four above and four below the plane of the Ln_4 fragment). The four remaining terminal ONep ligands radiate

(16) Evans, D. F. *J. Chem. Soc.* **1959**, 2003.
(17) Live, D. H.; Chan, S. I. *Anal. Chem.* **1970**, *42*, 791.
(18) Schubert, E. M. *J. Chem. Ed.* **1992**, *69*, 62.

Table 2. Metrical Data for **1**−**16**

Ln	La(**3**)[8a]	Ce (**4**)[8b]	Pr (**5**)	Nd(**6**)[8a]	Sm (**7**)	Eu (**8**)	Gd (**9**)	Tb (**10**)
*cation size[4]	1.032	1.01	0.990	0.983	0.958	0.947	0.938	0.923
Ln−H−C (cm^{-1})	2688	2687	2692	2692	2697	2697	2697	2697
Ln−Ln (Å)	3.85	3.81	3.78	3.74	3.69	3.66	3.68	3.61
Ln−$(OR)_{term}$ (Å)	2.16	2.14	2.12	2.14	2.09	2.08	2.10	2.06
Ln−(μ-OR) av (Å)	2.40	2.38	2.37	2.34	2.32	2.30	2.32	2.28
Ln−O−C_{term} (deg)	162.4	165.0	163.6	163.9	161.2	162.1	159.6	160.8
H-bond Ln−μO−C (deg)		106.3	120.0		122.6	107.7	124.9	124.2
H-bond Ln−C (Å)		3.13	3.29		3.30	3.0	3.34	3.28
Ln−μO−C (deg)		136.1	146.6		138.5	134.3	132.1	136.5
Ln−C (Å)		3.54	3.60		3.45	3.43	3.42	3.39

Ln	Dy (**11**)[6]	Ho (**12**)	Y (**2**)	Er (**13**)	Tm (**14**)	Yb (**15**)	Lu (**16**)	Sc (**1**)
cation size	0.912	0.901	0.9	0.89	0.88	0.868	0.861	0.745
Ln−H−C(cm^{-1})	2700	2700	2699	2701	2701	2702	2702	2698
Ln−Ln (Å)	3.58	3.55	3.56	3.53	3.51	3.49	3.46	3.28
Ln−$(OR)_{term}$ (Å)	2.04	2.03	2.04	2.03	2.02	2.01	2.00	1.89
Ln−(μ-OR) av (Å)	2.26	2.25	2.25	2.25	2.23	2.23	2.21	2.10
Ln−O−C_{term} (deg)	161.4	160.7	160.8	160.4	159.6	159.7	160.4	156.8
H-bond Ln−μO−C (deg)	107.2	125.7	126.1	119.5	121.3	133.5	120.9	113.0
H-bond Ln−C (Å)	3.03	3.28	3.28	3.19	3.25	3.35	3.17	3.01
Ln−μO−C (deg)	124.2	132.0	150.0	146.1	145.7	145.6	145.1	132.8
Ln−C (Å)	3.27	3.29	3.63	3.49	3.53	3.47	3.46	3.25

Table 3. $^{13}C\{^1H\}$ NMR Spectra of **1**−**3** in toluene-d_8

compd	$OCH_2C(CH_3)_3$	$OCH_2C(CH_3)_3$	$OCH_2C(CH_3)_3$
1	81.0	33.3	27.5, 26.8
2	79.7	33.1	27.2, 26.5
3	79.9	33.2	27.6, 26.7

outward from each metal center. Each metal is pentacoordinated and adopts a distorted square-based pyramidal geometry with a terminal alkoxide ligand occupying the apical position. Figure 1 shows a plot of the general structural unit observed for **1**−**16** using Gd as a representative member of the series. Table 2 lists some of the metrical data for **1**−**16**. The similarity in the structure adopted by all members of this family of compounds is truly surprising, since the 0.28 Å change in cation radius[4] was expected to result in significant differences within the coordination environment around the metal centers as the 4f-series is traversed.[9] The preservation of the same molecular asymmetric unit as the entire 4f-series is traversed has *not* previously been observed, and in this case it also extends to the group 3 cations.

The bond distances noted in Table 2 reflect the systematic trends that might be expected based on ionic radius considerations. Figure 2 shows a plot of the central void size versus the radii size of **1**−**16**. The Ln−Ln separations systematically decrease from 3.85 to 3.28 Å in proceeding from La to Lu and on to Sc which is a change of <0.5 Å, surprisingly, without any change in the overall structural arrangement. Terminal Ln−O distances span the range 2.16 Å (La, av value) to 1.89 Å (Sc) (with an overall average distance of 2.06 Å) which are in line with literature reports.[6,8,19] Only the Pr and Gd metrical data fall outside of this trend, attributable to the ESDs of the final structure solution in these instances. The average Ln−O distances recorded for the μ-ONep ligands are slightly longer, as expected, than the terminal distances and range from 2.40 (La) to 2.10 (Sc) Å with an average value for all of the cations of 2.28 Å. One notable feature of these molecules is the relatively close approaches of several bridging methylene carbon atoms to the metal centers, resulting in a distortion and asymmetry in some of the bridging metal−oxygen bonds. Ln−C−H distances were found to span from 3.01 (Sc) to 3.34 (Gd) Å. In contrast the non-H-bound Ln−C−H distances range from 3.25 (Sc) to 3.63(Y) Å. This was interpreted as an agostic interaction between the metals in question and the methylene group C−H bonds of *one* of the bridging ONep ligands along each metal axis. This interaction is also reflected in the angular variations of these compounds. The internal Ln−(μ-O)−C angles av 119° for the bridging ligands supporting agostic interactions versus 139° in the cases of the nonagostic μ-ONep ligand sets. The av Ln−O−C angles within the terminal alkoxide ligands span the range 162.4° (La) to 156.8° (Sc), typical for this general class of compounds.[6,8,19] The systematic variations demonstrated for this unique family of isostructural compounds highlight the potential utility of using this general homoleptic structural class of complexes for the exploration of fine-tuned, tailored materials. A few novel aspects of these compounds should be mentioned. While the aryloxide $Ln(OR)_x$ (x = 2 or 3) are typically crystallographically available, the number of alkyl derivatives for this family of compounds is scarce. For this series, compounds **1**, **5**, **9**, **12**, **13**, **14**, and **16** are the first examples of crystallographically characterized alkyl alkoxides reported in the Cambridge Data Base (2006). In fact for Tb, **10** is the first report of a $Tb(OR)_x$ of any kind reported.

FTIR Spectroscopy. The FTIR spectrum of each sample revealed the absence of any NR_2 stretches, which were replaced by the standard ONep ligand features, indicating full exchange of the amides with the alkoxide ligands in the products. Also observed in the spectra of **1**−**16** was a series of C−H (Ln−H−C) stretches between 2688−2692 cm^{-1} which are significantly reduced in value from standard aliphatic C−H bonds.[20] The observed frequencies are

(19) Wei, X.; Ming, L. J. *Inorg. Chem.* **1998**, *37*, 2255.

(20) Nakamoto, K. *Infrared and Raman Spectra of Inorganic and Coordiantion Compounds*, 5th ed.; John Wiley & Sons, Inc.: 1997.

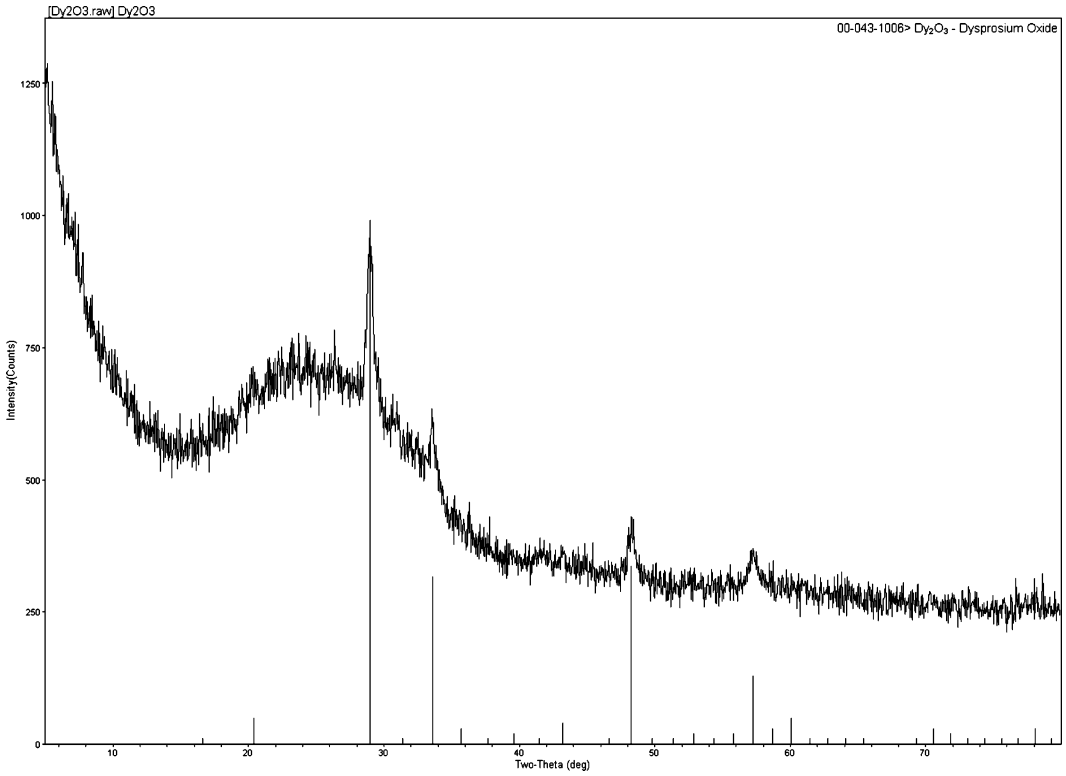

Figure 3. MicroXRD of Dy_2O_3 after heat treatment. Ideal pattern shown at bottom of spectrum.

consistent with the literature reported compounds[6,8] (see Table 2). As Table 2 reveals there is a general tendency toward increasing stretching frequency of these C−H bonds as the ionic radius of the trivalent ion decreases (i.e., the C−H bond strength appears to increase as the metal ion radius decreases). The reason for this phenomenon may simply be a result of steric constraints; however, this is highly speculative at this point. Further analysis of this issue via theoretical computation and neutron diffraction investigations are underway to fully understand the *detailed* nature of these M−H−C interactions.[21] Nonetheless, both the IR and X-ray data support agostic interactions within the entire series for **1**−**16**.

NMR Spectroscopy. Further NMR studies were undertaken to explore if these agostic interactions were maintained in solution. NMR data could not be collected for most of these compounds due to their paramagnetism; however, the group 3 systems are diamagnetic and therefore amenable to study via NMR spectroscopic methods. The Sc, (**1**) Y (**2**), and La (**3**) systems were therefore chosen as systems spanning the various "regions" of ionic radii investigated here. The room temperature ^{1}H NMR spectra reveal the presence of ONep ligands; however, the resonances are very broad due to coincidental overlap of the terminal and bridging ligands and/or rapid exchange processes in operation. ^{13}C NMR spectra were obtained since it was thought that these spectra might potentially exhibit reduction in $^1J_{C-H}$ coupling constants as a result of the agostic interactions that appear to be present in the solid-state structures. For **1**−**3**, $^{13}C\{^1H\}$ spectroscopy revealed the presence of two types of ONep ligands in an ∼1:2 ratio. These data are consistent with the solid-state structure in which there are two μ-ONep and one terminal ONep ligand. This observation also rules out dynamic (bridge-terminal) exchange involving all 12 alkoxide ligands. The two different types of bridging ligand quite likely possess similar chemical shift values for the methylene carbon resonances and therefore coincidentally overlap. The $^{13}C\{^1H\}$ data for these three species are tabulated in Table 2. Unfortunately the insolubility of these compounds at lower temperature precluded the collection of meaningful data concerning the nature of these interactions, also precluding a better understanding of any dynamic process that may be in operation within this series of molecules in solution.

Magnetic Susceptibility Measurements. In an effort to determine if there were any magnetic interaction between the four metal sites in these compounds magnetic susceptibility measurements were undertaken in solution. The NMR Evans' method was employed wherein select precursors were dissolved in tol-d_8 doped with 1% TMS. As expected, for the diamagnetic compound **1** and **2**, no magnetic susceptibility was noted. Compounds **3**, **6**, and **13** had a μ_{ett} of 0, whereas **7** and **15** had μ_{eff} of 0.3 and 1.14, respectively. While there are few reports on the magnetic susceptibility of lanthanide amine phenol nitrates that range from 7.88 to 3.33 μ_B),[22−24]the μ_B noted in this report for homoleptic [Ln(μ-ONep)$_2$(ONep)]$_4$ are an order of magnitude smaller.

(21) Gordon, J. C.; Hay, P. J.; Poli, R. Unpublished work.

(22) Westin, L. C.; Kritikox, M.; Caneschi, A. *Chem. Commun.* **2003**, 1012.
(23) Liu, S.; Gelmini, L.; Rettig, S. J.; Thompson, R. C.; Orvig, C. *J. Am. Chem. Soc.* **1992**, *114*, 6081.
(24) Wang, R.; Selby, H. D.; Liu, H.; Carducci, M. D.; Jin, T.; Zheng, Z.; Anthis, J. W.; Staples, R. J. *Inorg. Chem.* **2002**, *41*, 278.

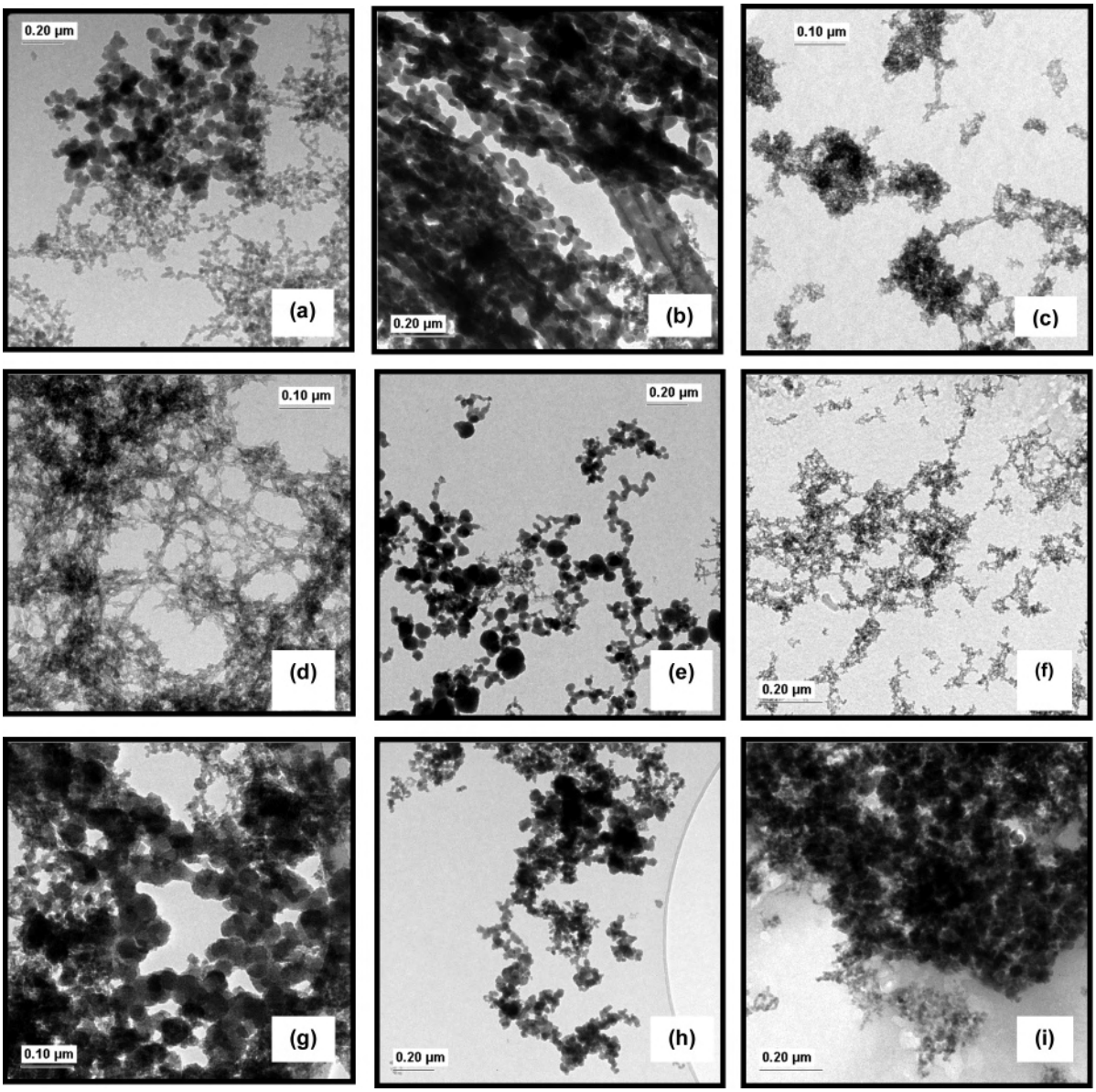

Figure 4. TEM images of the various Ln_2O_3 nanomaterials generated. TEM images of Ln_2O_3 where Ln = (a) Sc, (b)Yb, (c) Er, (d) Y, (e) Dy, (f) Gd, (g) Eu, (h) Pr, and (i) Ce (smallest cation to largest).

Nanoscale Ceramic Oxides. Representative members of this family of cations were chosen to investigate the hydrolytic behavior of these complexes, including Sc (**1**), Y(**2**), Ce (**4**), Pr (**5**), Eu (**8**), Gd (**9**), Dy (**11**), Er (**13**), and Yb(**15**). These precursors were selected so that we could investigate the entire series without necessarily generating each Ln_2O_3 nanoceramic phase. These tetrameric clusters were dissolved in toluene and injected into a refluxing mixture of 1-methylimidazole and water (MeIm:H_2O = 14.5: 0.5) This route has been previously exploited in our laboratory for the production of high quality nanoparticles of $Co(OH)_2$ disks and ZnO rods.[14,15] In each case there was a noticeable color change and a precipitate formed instantaneously. The powders were transferred to a quartz slides by taking a slurry of the Ln nanoparticles in isopropyl alcohol and allowing a single drop of this solution to dry in air, over time. XRD investigations revealed the powders were amorphous; however, TGA/DTA investigations of the metalorganic precursor indicated that crystallization occurs above ~1000 °C. Therefore, the powders were calcined at 1000 °C for 2 h. Analyses of the heated nanoparticles via micro-XRD revealed them to be nanocrystalline Ln_2O_3. Figure 3 shows a representative spectrum of the XRD powder pattern of Ln_2O_3 materials generated from **11**.

It was of interest to determine the size and morphological features of these materials. Therefore, TEM images were obtained which are shown in Figure 4. Polydisperse nanoceramic material was produced in each case. Specifically, for **1**, irregular particles ranging from 20 to 100 nm in size were observed. The larger particles consist of agglomerations of nanoparticles as if often noted for ceramic nanomaterials (this observation of the larger particles consisting of agglomerates of nanocrystallites is consistent throughout this series). Under the reaction conditions employed, as the cation radius increases, (i.e., **15**), the individual particles become more uniform with a size of ~8 nm. These also appear to

fuse together to create rodlike features. As the ionic radius is further increased in **13**, **2**, and **9**, a lacey network is observed consisting of uniform nanoparticles on the order of 8, 3, and 5 nm, respectively. Larger cations exhibit a mixture of small and larger particles: **11** (~8−121 nm), **8** (6−25 nm), and **5** (33−78 nm). The largest cation, **4**, yields nanoparticles below 10 nm in size. Additional studies are underway to exploit the various "cation-induced" morphological changes noted above. This control is only available due to the isostructural nature of the 16 compounds isolated from this study and the systematic variations wrought from the lanthanide contraction.

In order to characterize the luminescent properties of these materials, the UV−vis spectra of the precursors **1**−**3**, **5**, and **11** and their respective nanoparticles were obtained. The spectra recorded for **1**−**3**, **5**, and **11** were in agreement with each other and the spectrum recorded for H-ONep. In contrast, the nanoparticles display a significantly varied spectrum wherein a broad multiplet was observed around 220 nm followed by a broader and smaller feature around 255 nm: compound (peaks, nm)) - **1** (219, 259), **2 (**222, 257), **5 (**222, 241), **11** (219, 254). Further, characterization via photoluminescence (PL) measurements were also attempted for the same samples. Surprisingly, the spectra of these samples were *not* in agreement with the literature description of Ln_2O_3 nanoparticles.[17] In this report, these materials were synthesized from commercially available LnX_3 (X=Cl) precursors. The use of LnX_3 precursors in our hands under similar conditions yielded materials that produced identical PL measurements as the literature reports but were found by XRD analysis to be "$Ln(OH)_2Cl$" and *not* Ln_2O_3.[17] Each Ln_2O_3 sample analyzed exhibited a single feature. Upon further analysis of these spectra, it was found that the observed feature was a false "emission" band (i.e., a second-order Rayleigh feature, observable at twice the wavelength of the excitation beam in each case). This is a harmonic effect of the excitation beam and the excitation monochromator and not a true reflection of the emission properties of the Ln_2O_3 nanomaterials of interest. Future work on obtaining the true PL measurement of Ln_2O_3 will focus on selective scans around the emission energy.

Conclusion

We have successfully synthesized and characterized homoleptic ONep derivatives of the entire Ln series and their group 3 congeners. Surprisingly, *each* of the 16 cations investigated which represent a change in radii of ~0.28 Å were found to adopt an isostructural, tetrameric $[Ln(\mu\text{-}ONep)_2(ONep)]_4$ structure. NMR spectra of representative systems indicate this structural motif is maintained in solution. A number of these $Ln(OR)_3$ (**1**, **5**, **9**, **12**, **13**, **14**, and **16**) are the first examples of crystallographically characterized alkyl alkoxides reported to date and the first alkoxide reported for Tb (**10**). Agostic interactions involving methylene groups of the μ-ONep ligands were observed in the metrical data for each structure and correlated to a (varying) stretch feature in the FTIR spectrum. Nanomaterials generated from select cations of these 16 *iso*-structural precursors produced a variety of nanoparticle morphologies, ranges from spheres to rods. The only variable was the cation present in the precursor with the larger cations tend to form a more rodlike material under the conditions employed. Additional work is underway to control the shape of the nanoparticles formed and understand the nature of the Ln−H−C bonding interaction noted for each complex[21] as well as determine the "true" PL behavior of these Ln_2O_3 materials.

Acknowledgment. For support of this research, the authors thank the Office of Basic Energy Science and the U.S. Department of Energy under Contract DE-AC04-94AL85000. Sandia is a multiprogram laboratory operated by Sandia Corporation, a Lockheed Martin Company, for the United States Department of Energy. Los Alamos National Laboratory is managed and operated by Los Alamos National Security, LLC under Contract No. DE-AC52-06NA25396.

Supporting Information Available: CIF files. This material is available free of charge via the Internet at http://pubs.acs.org. The CIF files can also be accessed through the Cambridge Crystallographic Data Base.

IC070253U